Submitted to *Chem. Commun.*, July 2012

ELECTRONIC SUPPLEMENTARY INFORMATION

Bifunctional Luminescence Single-Ion Magnet: Towards Correlation Between Luminescence Studies and Magnetic Slow Relaxation Processes.

Jérôme Long,*[a] Rémi Vallat,[a] Rute A. S. Ferreira,[b] Luis D. Carlos,[b] Filipe A. Almeida Paz,[c] Yannick Guari[a] and Joulia Larionova[a]

[a] *Institut Charles Gerhardt Montpellier, UMR 5253, Chimie Moléculaire et Organisation du Solide, Université Montpellier II, Place E. Bataillon, 34095 Montpellier cedex 5, France.*

[b] *Physics department, CICECO, University of Aveiro, 3810 -193 Aveiro, Portugal.*

[c] *Department of Chemistry, CICECO, University of Aveiro, 3810 -193 Aveiro, Portugal.*

EXPERIMENTAL SECTION

Syntheses:

All experiments were carried out under aerobic conditions. The lanthanide nitrate salts were purchased from ABCR. All the solvents in these experiments were analytical grade.

The ligand H_2L (H_2 = N,N'-bis(3-methoxysalicylidene)-1,2-diaminoethane) has been synthesized according to a well-established procedure from the literature.[1] The [ZnL(H_2O)] complex has been synthesized by refluxing $Zn(OAc)_2{\cdot}2H_2O$ with H_2L in ethanol according to the procedure from the literature.[2]

Synthesis of [ZnDy(L)(NO_3)$_3$(H_2O)] (**1**) and [Zn(H_2O)(L)Tb(NO_3)$_3$]·CH_3CN (**2**).

The stochioemetric reaction between [ZnL(H_2O)] (0.78 mmol, 0.320 g) and $Ln(NO_3)_3{\cdot}6H_2O$ (0.78 mmol) in 20 mL of acetonitrile gives a clear yellow solution upon heating. Slow diffusion of diethyl-ether yields to the formation of yellow crystals which are air stable over a period of several weeks. Yield = 67 % (ZnDy); 68 % (ZnTb). Elemental analysis cald for $ZnDyC_{18}H_{20}N_5O_{14}$ (exp.): C 28.51 (28.42), H 2.66 (2.86), N 9.23 (9.20). Elemental analysis cald for $ZnTbC_{20}H_{23}N_6O_{14}$ (exp.): C 30.05 (30.11), H 2.90 (3.14), N 10.51 (10.13).

Single-Crystal X-ray Diffraction Studies

Single-crystals of compounds [Zn(NO_3)(L)Dy(NO_3)$_2$(H_2O)] (**1**) and [Zn(H_2O)(L)Tb(NO_3)$_3$]·CH_3CN (**2**) (where H_2L = *N*,*N*'-bis(3-methoxysalicylidene)-1,2-diaminoethane) were manually harvested from the crystallization vials and mounted on glass fibers.[3] Data were collected at 173(2) K on an Oxford Instruments Xcalibur Sapphire-2 charge-coupled device (CCD) area-detector diffractometer with a (Mo K_α graphite-monochromated radiation, λ = 0.71073 Å) controlled by the Crysalis^{Pro} software package.[4] Images were processed using the same general software package and data were corrected for absorption (using spherical harmonics) by the multi-scan semi-empirical method implemented in SCALE3 ABSPACK of Crysalis^{Pro}.[5]

Structures were solved employing the Patterson algorithm implemented in the software package SHELXS-97.[4] This approach allowed the location of the two distinct metallic centres composing each individual complex of compounds **1** and **2**. All remaining non-hydrogen atoms were directly located from difference Fourier maps calculated from successive full-matrix least squares refinement cycles on F^2 using SHELXL-97.[6b, 7] In compound **2**, the diethylene group belonging to the chelating *N*,*N*'-bis(3-methoxysalicylidene)-1,2-diaminoethane organic ligand was found to have positional disorder for the carbon atoms. The two locations were refined with fixed rates of occupancy of 0.75 and 0.25 which were found from prior unrestrained refinement studies. Nevertheless, all non-hydrogen atoms in both structures have been successfully refined using anisotropic displacement parameters.

The crystallographically independent hydrogen atoms associated with the sole coordinated water molecule in each compound were directly located from difference Fourier maps and were included in the final structural models with the O–H and H···H distances restrained to 0.95(1) and 1.55(1) Å, respectively, so to ensure a chemically reasonable geometry for this chemical moiety. The isotropic thermal displacement parameter (U_{iso}) of the hydrogen atoms were fixed at 1.5×U_{eq} of the oxygen atom to which they are attached.

Despite the location of most of the hydrogen atoms bound to carbon could be discerned from difference Fourier maps at the later stages of the refinement procedure, these were instead placed at idealized positions using appropriate *HFIX* instructions in SHELXL: *43* for the aromatic and –CH=N– carbons; *23* for the $–CH_2–$ groups; *137* for the terminal $–CH_3$ moieties. All these atoms have been included in subsequent refinement cycles in riding-motion approximation with U_{iso} fixed at 1.2 (for the former groups) or $1.5\times U_{eq}$ (only for the latter moieties) of the carbon atom to which they are attached, respectively.

The last difference Fourier map synthesis showed: for **1**, the highest peak (0.418 $eÅ^{-3}$) and deepest hole (-0.370 $eÅ^{-3}$) located at 0.69 Å from C6 and 0.74 Å from Dy1, respectively; for **2**, the highest peak (0.424 $eÅ^{-3}$) and deepest hole (-0.358 $eÅ^{-3}$) located at 0.65 Å from C6 and 0.99 Å from Zn1, respectively.

Information concerning crystallographic data collection and structure refinement details is summarized in Table S3. Tabulated data on the geometrical aspects of the coordination environments of the metallic centers for both compounds, and of the O−H···(N,O) hydrogen bonding interactions present in both crystal structures are provided as Tables S4 to S9. Structural drawings have been created using the software package Crystal Impact Diamond.[8]

Crystallographic data (including structure factors) for the two structures reported in this communication have been deposited with the Cambridge Crystallographic Data Centre as supplementary publication nos. CCDC-887656 (for **1**) and -887655 (for **2**). Copies of the data can be obtained free of charge on application to CCDC, 12 Union Road, Cambridge CB2 2EZ, U.K. FAX: (+44) 1223 336033. E-mail: deposit@ccdc.cam.ac.uk.

Magnetic Measurements

Magnetic susceptibility data were collected with a Quantum Design MPMS-XL SQUID magnetometer working between 1.8 – 350 K with the magnetic field up to 7 Tesla. The data were corrected for the sample holder and the diamagnetic contributions calculated from the Pascal's constants (*Theory and Applications of Molecular Paramagnetism*, Eds. Boudreaux, E. A. L.; Mulay, L. John Wiley Sons, New York, 1976).

Photoluminescence Measurements

The photoluminescence properties were investigated, at room temperature, using a modular double grating excitation spectrofluorimeter with a TRIAX 320 emission monochromator (Fluorolog-3, Horiba Scientific) coupled to a R928 Hamamatsu photomultiplier, using a front face acquisition mode. The excitation source was a 450 W Xe arc lamp. The emission spectra were corrected for detection and optical spectral response of the spectrofluorimeter and the excitation spectra were corrected for the spectral distribution of the lamp intensity using a photodiode reference detector. The room temperature emission decay curves of the $^5D_4$ (Tb^{3+}) level were monitored using a modular double grating excitation spectrofluorimeter with a TRIAX 320 emission monochromator (Fluorolog-3, Horiba Scientific) coupled to a R928 Hamamatsu photomultiplier employing a pulsed Xe–Hg lamp (6 μs pulse at half width and 20–30 μs tail). The emission decay curves of the $^4F_{9/2}$ (Dy^{3+}) excited state were monitored with a Fluorolog TCSPC spectrofluorometer (Horiba Scientific) coupled to a TBX-04 photomultiplier tube module (950 V), 200 ns time-to-amplitude converter and 70 ns delay. The exciting source was a Horiba-Jobin-Yvon pulsed diode (NanoLED-390, peak at 390 nm, 1.2 ns pulse duration, 1 MHz repetition rate, and 150 ns synchronization delay).

Figures S1-S14

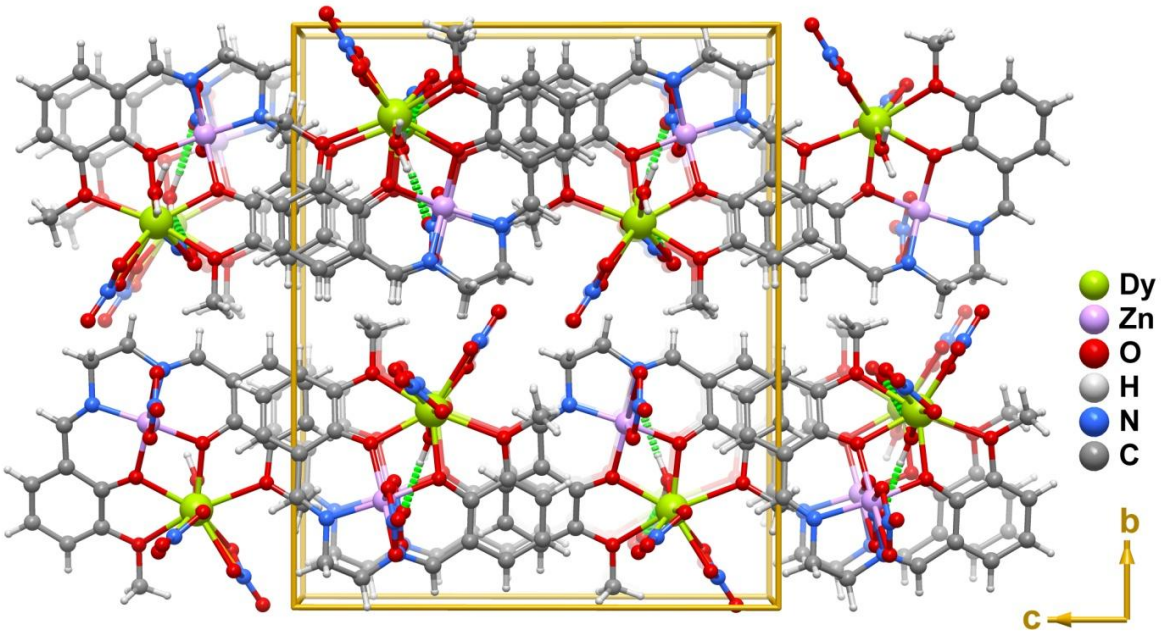

Figure S1. Crystal packing of compound $[Zn(NO_3)(L)Dy(NO_3)_2(H_2O)]$ (**1**) viewed in perspective along the [100] direction of the unit cell. O−H···O hydrogen bonding interactions connecting adjacent complexes are represented as dashed green lines. For geometrical details on the represented hydrogen bonds see Table S8.

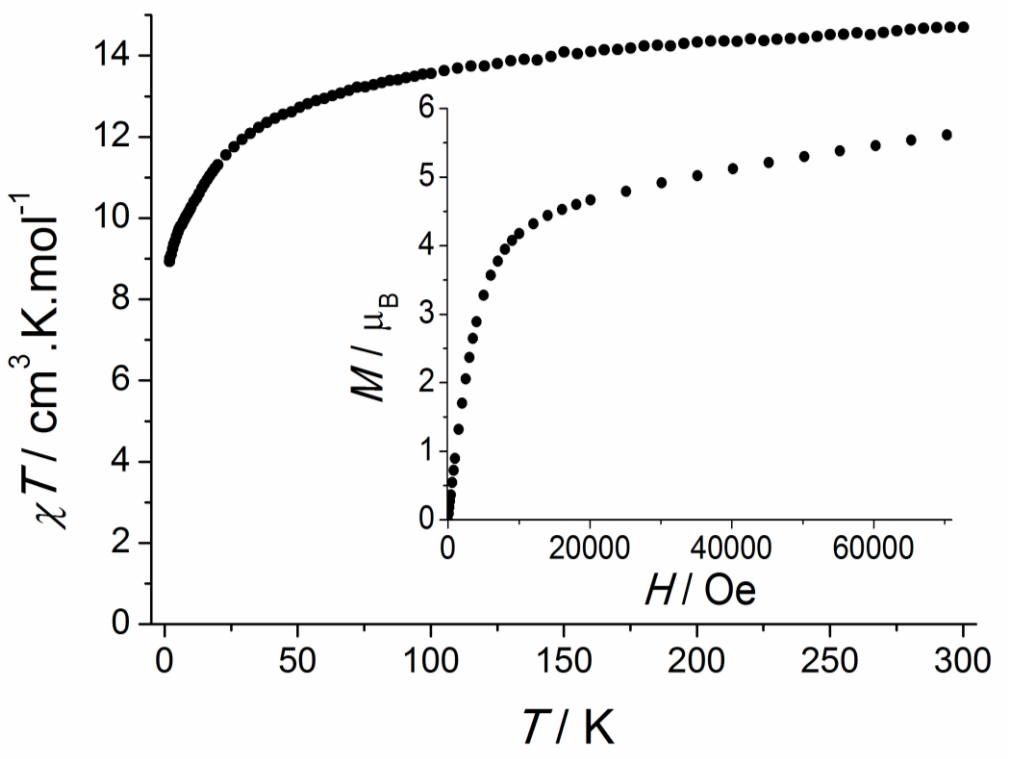

Figure S2. Temperature dependence of χT under a 1000 Oe DC field for $[Zn(NO_3)(L)Dy(NO_3)_2(H_2O)]$ (**1**). Inset: Field dependence of the magnetisation at 1.8 K.

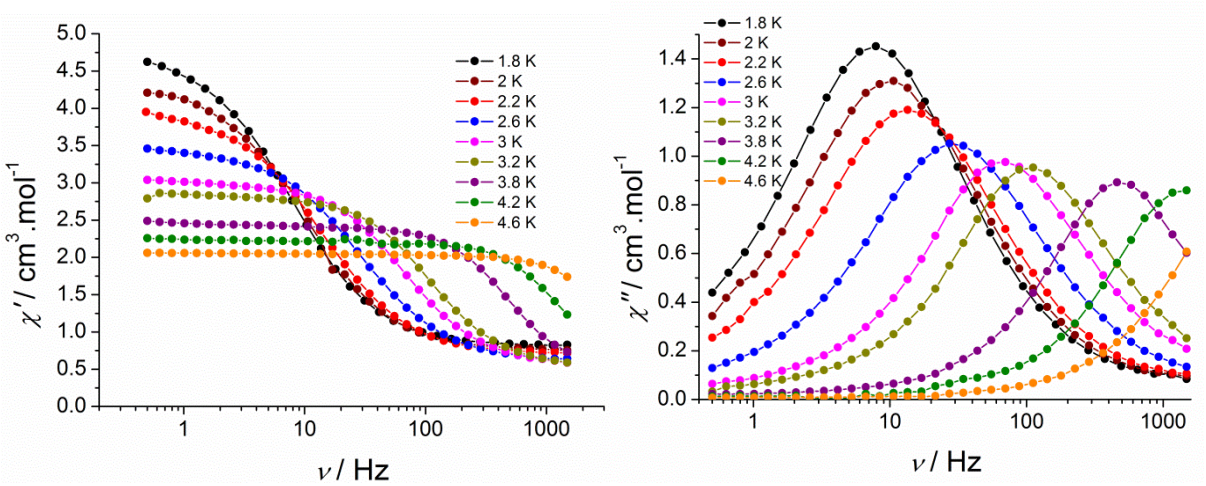

Figure S3. Frequency dependence of the in-phase and out-of-phase susceptibilities for [Zn(NO$_3$)(*L*)Dy(NO$_3$)$_2$(H$_2$O)] (**1**) under a 900 Oe DC field value for temperature ranging from 1.8 to 4.6 K.

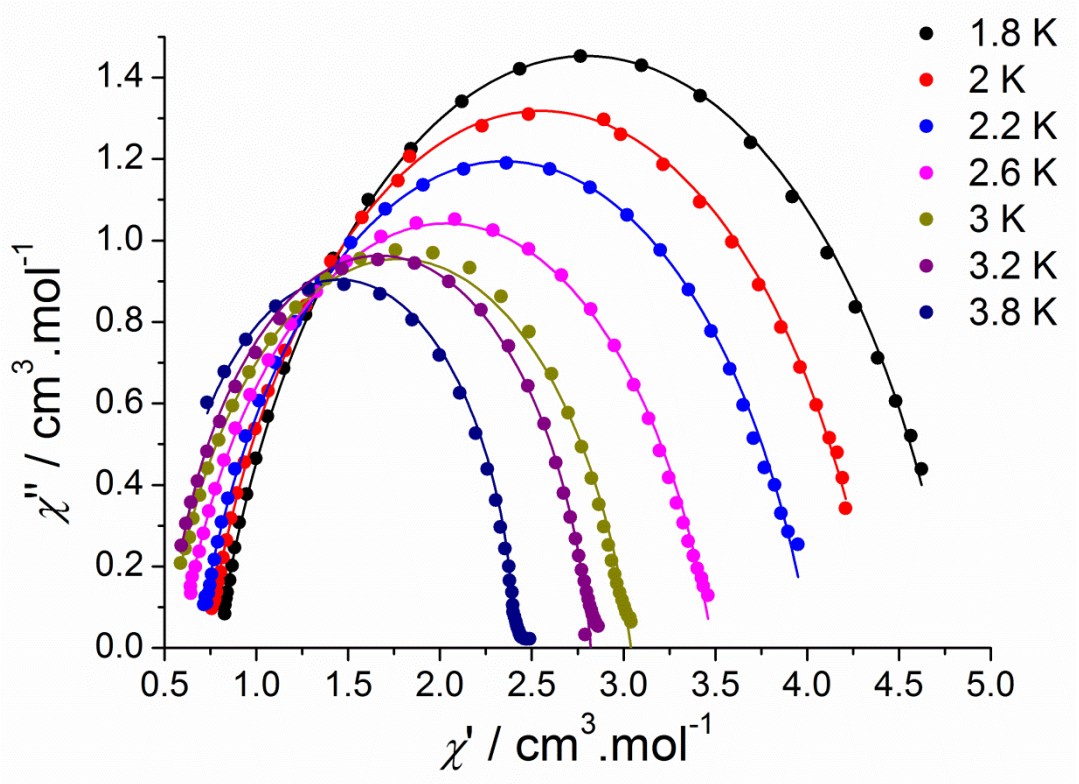

Figure S4. Cole-Cole (Argand) plot for [Zn(NO$_3$)(*L*)Dy(NO$_3$)$_2$(H$_2$O)] (**1**) obtained using the ac susceptibility data (900 Oe). The solid lines correspond to the best fit obtained with a generalized Debye model.

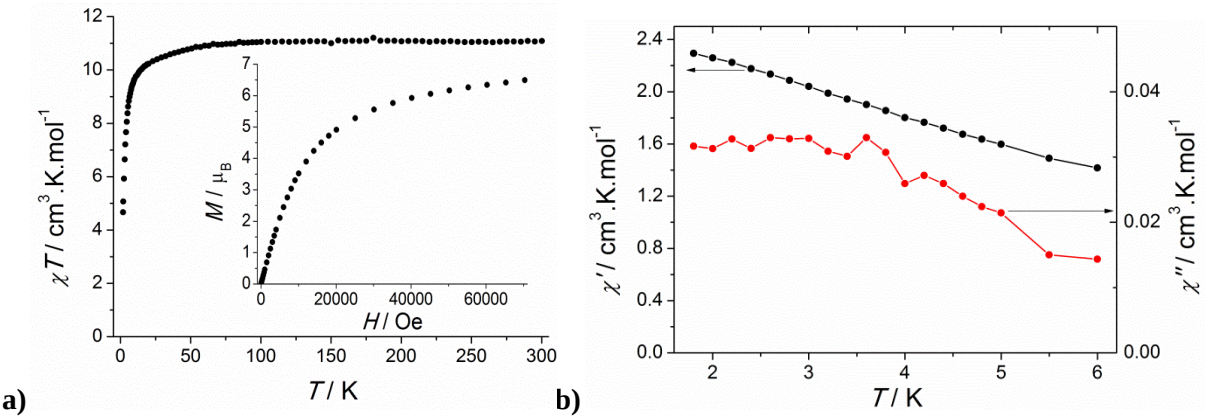

Figure S5. a) Temperature dependence of χT under a 1000 Oe DC field for $[Zn(H_2O)(L)Tb(NO_3)_3]\cdot CH_3CN$ (**2**). Inset: Field dependence of the magnetisation at 1.8 K; b) Temperature dependence of in-phase, χ', and out-of phase, χ'', components of the ac susceptibility for $[Zn(H_2O)(L)Tb(NO_3)_3]\cdot CH_3CN$ (**2**) performed at 999.87 Hz under a 1600 Oe DC field showing the absence of significant out-of-phase signal.

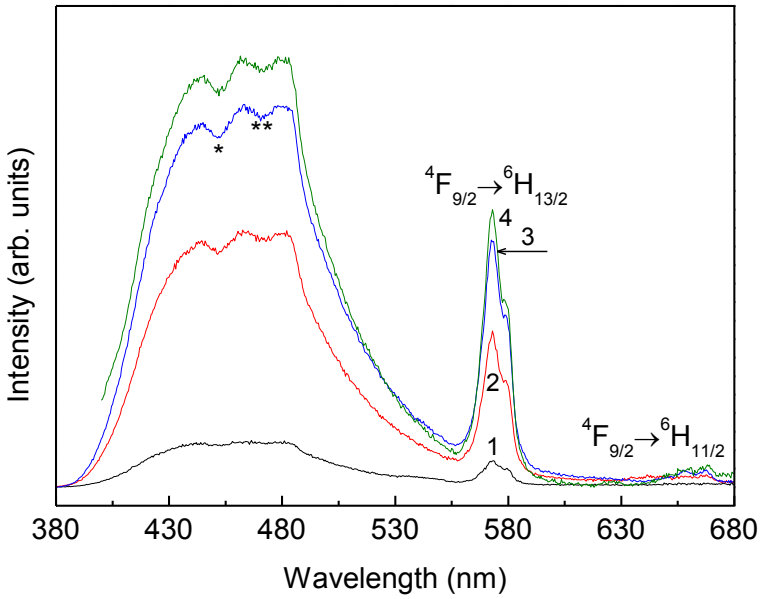

Figure S6. Emission spectra of [Zn(NO$_3$)(*L*)Dy(NO$_3$)$_2$(H$_2$O)] (**1**) excited at (1) 280, (2) 315-320, (3) 360 and (4) 380 nm. The (*) and (**) denote the Dy^{3+} $^4H_{15/2}\rightarrow{}^4I_{15/2}$, $^4I_{15/2}$ self-absorptions, respectively.

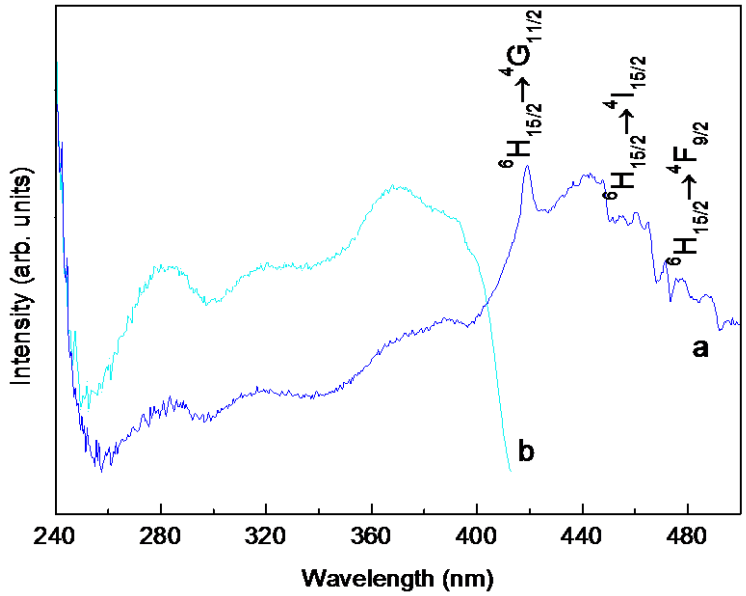

Figure S7. Excitation spectra of compounds [Zn(NO$_3$)(*L*)Dy(NO$_3$)$_2$(H$_2$O)] (**1**) monitored at 573 nm (a) and 460 nm (b).

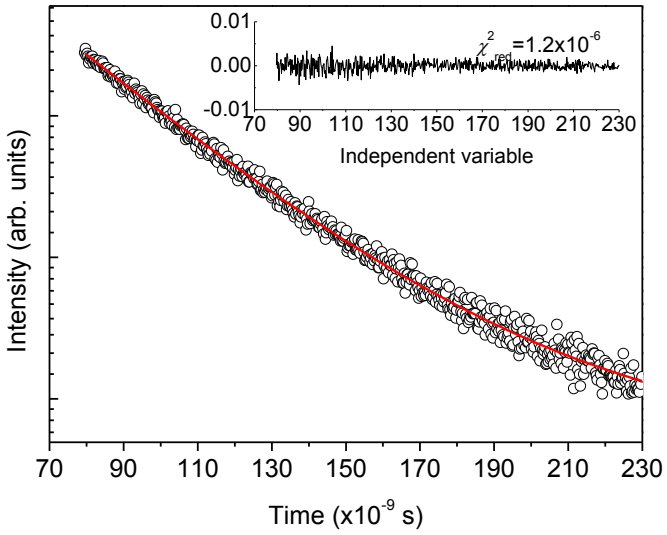

Figure S8. Emission decay curve of [Zn(NO$_3$)(*L*)Dy(NO$_3$)$_2$(H$_2$O)] (**1**) monitored at 573 nm and excited at 390 nm. The solid line represents the data best fit using a single exponential function. The inset shows the respective regular residual plot and the χ^2_{red} value for a better judgment of the fit quality.

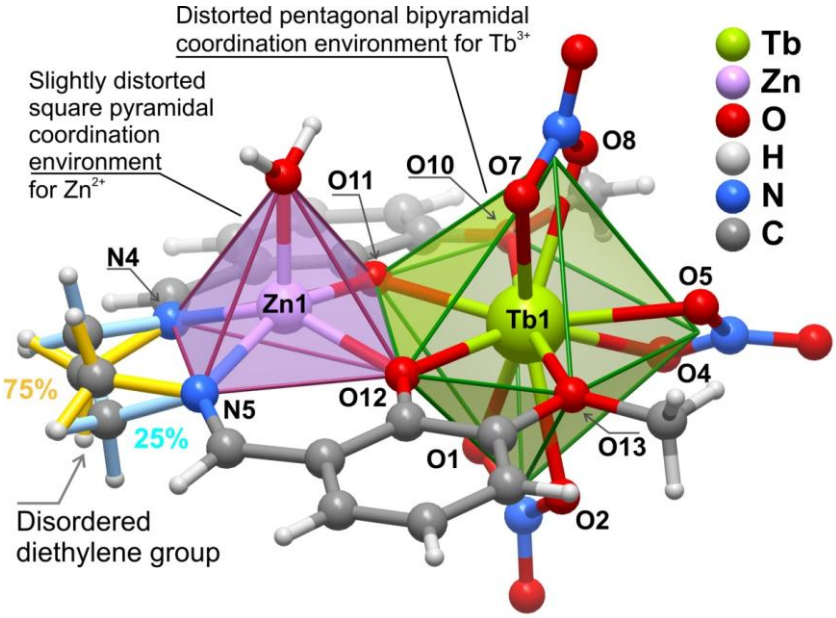

Figure S9. Mixed ball-and-stick and polyhedral representation of the dinuclear complex [Zn(H$_2$O)(*L*)Tb(NO$_3$)$_3$] present in compound **2**. For clarity, the coordination polyhedra of Zn^{2+} and Tb^{3+} are represented as translucent solid objects with the centers of gravity of the coordinated nitrato-*O*,*O*' being taken as a single coordination site. The atomic labelling scheme for all atoms composing the first coordination sphere of each metallic center is provided. For selected bond lengths and angles of the Zn^{2+} and Tb^{3+} coordination polyhedra see Tables S6 and S7, respectively.

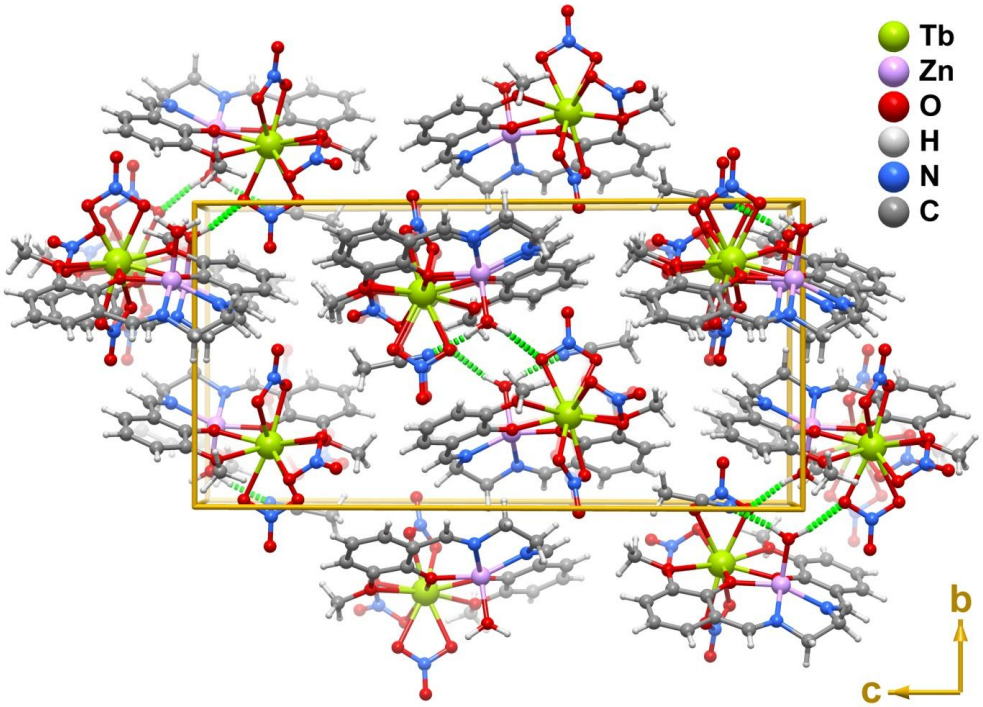

Figure S10. Crystal packing of compound $[Zn(H_2O)(L)Tb(NO_3)_3]\cdot CH_3CN$ (**2**) viewed in perspective along the [100] direction of the unit cell. O−H···(N,O) hydrogen bonding interactions connecting adjacent complexes and acetonitrile crystallization solvent molecules are represented as dashed green lines. For geometrical details on the represented hydrogen bonds see Table S9. Please note: for clarity, only the portion with 75% rate of occupancy of the disordered diethylene group (see Figure S8) is represented.

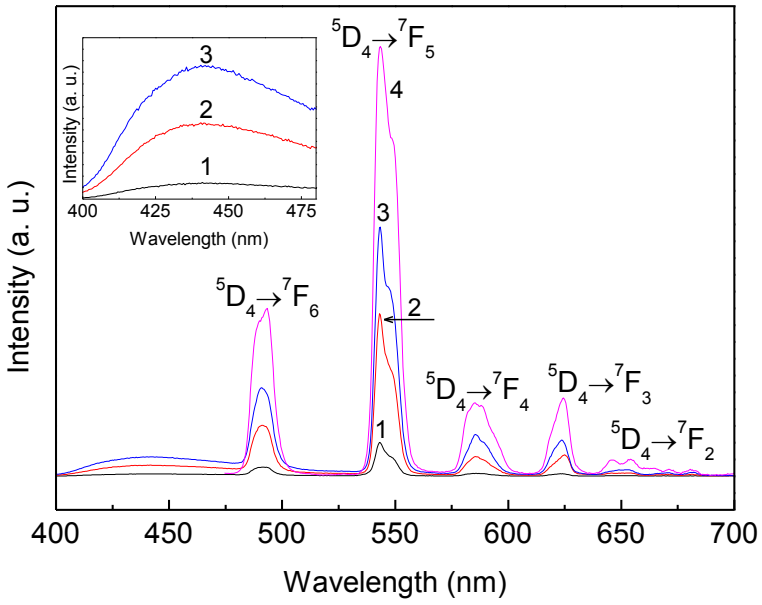

Figure S11. Emission spectra of $[Zn(H_2O)(L)Tb(NO_3)_3]$ (**2**) excited at (1) 280, (2) 315-320, (3) 360 and (4) 380 nm. The inset shows a magnification (×10) of the emission in the 400-480 nm range.

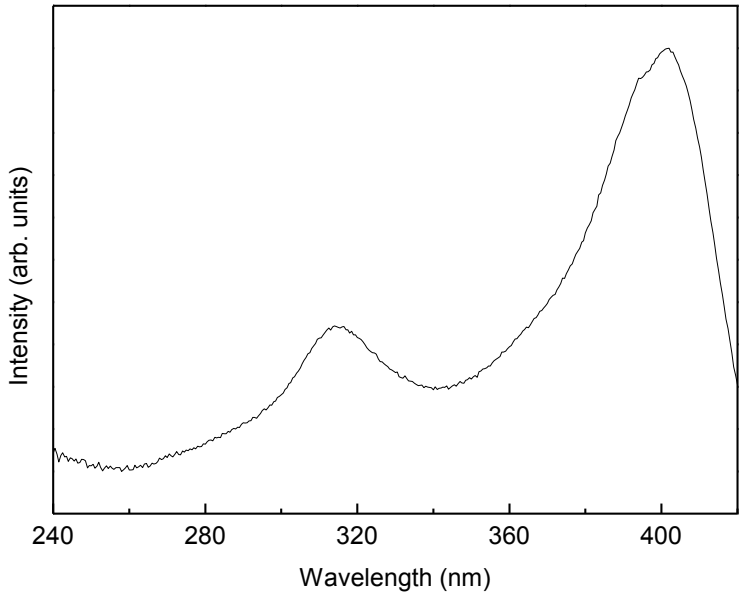

Figure S12. Excitation spectra of $[Zn(H_2O)(L)Tb(NO_3)_3]$ (**2**) monitored at 543 nm.

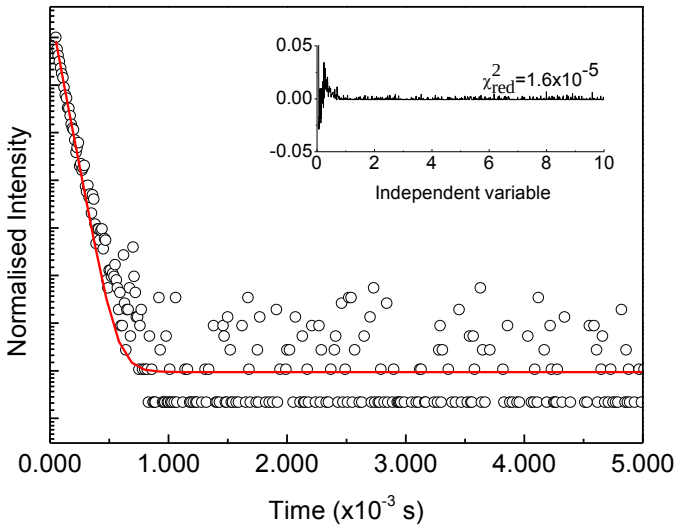

Figure S13. Emission decay curve of $[Zn(H_2O)(L)Tb(NO_3)_3]$ (**2**) monitored at 543 nm and excited at 315 nm. The solid line represents the data best fit using a single exponential function. The inset shows the respective regular residual plot and the χ^2_{red} value for a better judgment of the fit quality.

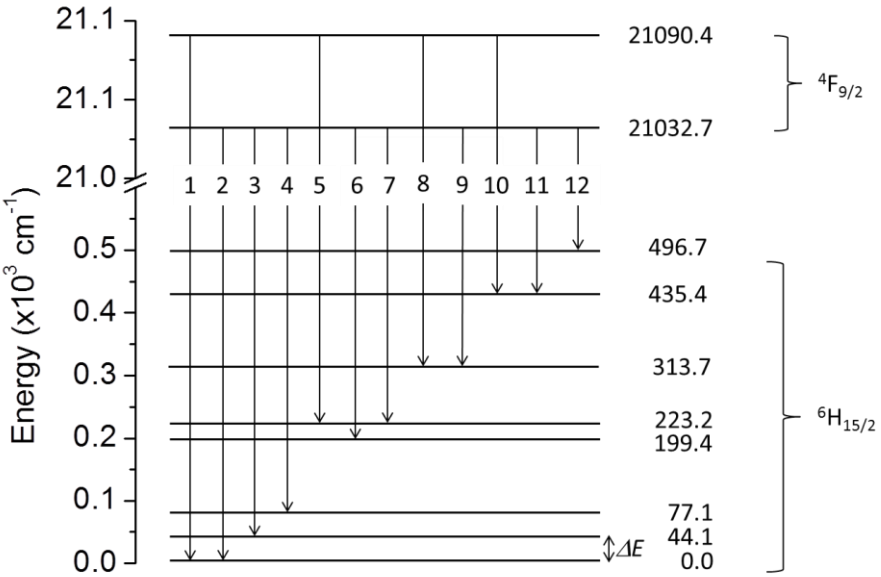

Figure S14. Schematic diagram of the radiative transitions between the Stark sublevels of the $^4F_{9/2}$ and $^6H_{15/2}$ multiplets of the Dy^{3+} ion.

Tables S1-S9

Table S1. Fitting of the Cole-Cole plots with a generalized Debye model for temperature ranging from 1.8 to 3.8 K.

T (K)	α	χ_S ($cm^3.\ mol^{-1}$)	χ_T ($cm^3.\ mol^{-1}$)
1.8	0.252	1.214	4.376
2.0	0.254	1.115	3.984
2.2	0.264	1.048	3.648
2.6	0.260	0.899	3.167
3.0	0.213	0.741	2.809
3.2	0.128	0.650	2.682
3.8	0.080	0.495	2.347

Table S2. Energy peak position (E, ±3.0 cm^{-1}) and full-width-at-half maximum (*fwhm*, cm^{-1}) of the $^4F_{9/2}\rightarrow{}^6H_{15/2}$ Stark components (identified from 1-10) determined from the experimental emission spectrum (acquired at 12 K and excited at 385 nm) best fit ($\chi^2_{red}=1.7\times10^{-3}$) using a 12-components Gaussian function for $[Zn(NO_3)(L)Dy(NO_3)_2(H_2O)]$ (**1**) .

Assignment*	***E***	***fwhm***
12	20536.0	80.0±4.8
11	20597.3	40.0±1.2
10	20650.5	40.0±1.2
9	20719.0	38.0±0.8
8	20784.1	31.5±1.1
7	20809.5	18.9±1.1
6	20833.3	24.9±1.1
5	20876.8	33.1±1.1
4	20955.6	30.0±6.0
3	20988.6	17.6±1.5
2	21032.7	20.9±2.5
1	21090.4	25.0±1.9

* The assignment is illustrated in Figure 4 and Figure S14.

Crystallographic Tables

Table S3. Crystal and structure refinement data for compounds **1** and **2**.

	1	**2**
Formula	$C_{18}H_{20}DyN_5O_{14}Zn$	$C_{20}H_{23}N_6O_{14}TbZn$
Formula weight	758.26	795.73
Temperature / K	173(2)	173(2)
Crystal system	Monoclinic	Monoclinic
Space group	$P2_1/n$	$P2_1/c$
a/Å	7.75620(16)	9.59761(16)
b/Å	19.2440(4)	11.88217(18)
c/Å	16.0150(3)	23.8362(4)
β/º	91.3111(18)	98.4800(16)
Volume/Å^3	2389.79(8)	2688.57(8)
Z	4	4
D_c/g cm^{-3}	2.108	1.966
μ(Mo-Kα)/mm^{-1}	4.190	3.582
F(000)	1484	1568
Crystal size/mm	0.22×0.10×0.02	0.18×0.16×0.11
Crystal type	Colourless plates	Colourless blocks
θ range	3.59 to 29.13	3.54 to 29.13
Index ranges	$-10 \le h \le 10$	$-13 \le h \le 13$
	$-26 \le k \le 26$	$-16 \le k \le 16$
	$-21 \le l \le 21$	$-32 \le l \le 32$
Reflections collected	41024	88541
Independent reflections	6424 (R_{int} = 0.0288)	7220 (R_{int} = 0.0254)
Data completeness	99.8%	99.8%
Data / parameters	6424 / 360	7220 / 406
Final R indices [I>2σ(I)][a,b]	$R1$ = 0.0163	$R1$ = 0.0159
	$wR2$ = 0.0339	$wR2$ = 0.0336
Final R indices (all data)[a,b]	$R1$ = 0.0201	$R1$ = 0.0182
	$wR2$ = 0.0348	$wR2$ = 0.0343
Weighting scheme[c]	m = 0.0116	m = 0.0088
	n = 1.8231	n = 2.0900
Largest diff. peak and hole	0.418 and -0.370 eÅ^{-3}	0.424 and -0.358 eÅ^{-3}

[a] $R1 = \sum \| |F_o| - |F_c| \| / \sum |F_o|$; [b] $wR2 = \sqrt{\sum \left[w\left(F_o^2 - F_c^2\right)^2 \right] / \sum \left[w\left(F_o^2\right)^2 \right]}$

[c] $w = 1/\left[\sigma^2\left(F_o^2\right) + \left(mP\right)^2 + nP \right]$ where $P = \left(F_o^2 + 2F_c^2\right)/3$

Table S4. Bond distances (in Å) for the two crystallographically independent metallic coordination environments present in compound [Zn(NO_3)(*L*)Dy(NO_3)$_2$(H_2O)] (**1**).

Dy1–O1	2.4497(13)	Zn1–O7	2.0595(13)
Dy1–O2	2.4324(14)	Zn1–O11	2.0294(12)
Dy1–O4	2.4456(13)	Zn1–O12	2.0035(12)
Dy1–O5	2.4961(13)	Zn1–N4	2.0327(15)
Dy1–O10	2.4907(12)	Zn1–N5	2.0376(15)
Dy1–O11	2.3081(12)		
Dy1–O12	2.2771(12)		
Dy1–O13	2.5376(12)		
Dy1–O1W	2.3268(13)		
Dy1–N1	2.8787(15)		
Dy1–N2	2.8812(15)		

Table S5. Bond angles (in degrees) for the two crystallographically independent metallic coordination environments present in compound $[Zn(NO_3)(L)Dy(NO_3)_2(H_2O)]$ (**1**).

O1–Dy1–O5	70.58(5)	O11–Dy1–N2	81.15(4)
O1–Dy1–O10	93.90(4)	O12–Dy1–O1	137.46(5)
O1–Dy1–O13	78.34(4)	O12–Dy1–O2	130.22(5)
O1–Dy1–N1	26.21(4)	O12–Dy1–O4	79.67(4)
O1–Dy1–N2	72.84(4)	O12–Dy1–O5	117.64(4)
O2–Dy1–O1	52.32(4)	O12–Dy1–O10	128.30(4)
O2–Dy1–O4	126.37(5)	O12–Dy1–O11	66.76(4)
O2–Dy1–O5	110.84(5)	O12–Dy1–O13	63.09(4)
O2–Dy1–O10	80.90(5)	O12–Dy1–O1W	76.51(5)
O2–Dy1–O13	80.32(5)	O12–Dy1–N1	140.66(4)
O2–Dy1–N1	26.11(4)	O12–Dy1–N2	98.02(4)
O2–Dy1–N2	123.48(4)	O13–Dy1–N1	78.40(4)
O4–Dy1–O1	75.36(5)	O13–Dy1–N2	103.07(4)
O4–Dy1–O5	51.69(4)	O1W–Dy1–O1	121.08(5)
O4–Dy1–O10	117.28(4)	O1W–Dy1–O2	69.05(5)
O4–Dy1–O13	78.27(4)	O1W–Dy1–O4	155.89(5)
O4–Dy1–N1	101.04(5)	O1W–Dy1–O5	146.61(5)
O4–Dy1–N2	26.10(4)	O1W–Dy1–O10	81.18(5)
O5–Dy1–O13	125.70(4)	O1W–Dy1–O13	87.64(5)
O5–Dy1–N1	90.60(4)	O1W–Dy1–N1	95.05(5)
O5–Dy1–N2	25.71(4)	O1W–Dy1–N2	164.38(5)
O10–Dy1–O5	66.27(4)	N1–Dy1–N2	98.20(4)
O10–Dy1–O13	160.61(4)		
O10–Dy1–N1	86.81(4)	O11–Zn1–O7	98.96(5)
O10–Dy1–N2	91.30(4)	O11–Zn1–N4	89.52(5)
O11–Dy1–O1	145.99(5)	O11–Zn1–N5	133.39(6)
O11–Dy1–O2	138.80(5)	O12–Zn1–O7	97.70(5)
O11–Dy1–O4	90.80(5)	O12–Zn1–O11	77.45(5)
O11–Dy1–O5	76.44(5)	O12–Zn1–N4	152.14(6)
O11–Dy1–O10	64.71(4)	O12–Zn1–N5	89.38(5)
O11–Dy1–O13	129.79(4)	N4–Zn1–O7	108.70(6)
O11–Dy1–O1W	83.26(5)	N4–Zn1–N5	81.80(6)
O11–Dy1–N1	151.44(4)	N5–Zn1–O7	127.26(6)

Table S6. Bond distances (in Å) for the two crystallographically independent metallic coordination environments present in compound $[Zn(H_2O)(L)Tb(NO_3)_3]\cdot CH_3CN$ (**2**).

Tb1–O1	2.4508(12)	Zn1–O11	2.0045(11)
Tb1–O2	2.4574(14)	Zn1–O12	2.0180(11)
Tb1–O4	2.4633(13)	Zn1–O1W	1.9876(12)
Tb1–O5	2.4817(13)	Zn1–N4	2.0418(14)
Tb1–O7	2.4635(12)	Zn1–N5	2.0263(14)
Tb1–O8	2.5540(13)		
Tb1–O10	2.6604(12)		
Tb1–O11	2.3422(11)		
Tb1–O12	2.3461(11)		
Tb1–O13	2.7273(12)		
Tb1–N1	2.8756(15)		
Tb1–N2	2.9099(14)		

Table S7. Bond angles (in degrees) for the two crystallographically independent metallic coordination environments present in compound $[Zn(H_2O)(L)Tb(NO_3)_3]\cdot CH_3CN$ (**2**).

O1–Tb1–O2	52.23(4)	O10–Tb1–O13	169.53(4)
O1–Tb1–O4	71.04(4)	O10–Tb1–N1	95.60(5)
O1–Tb1–O5	116.73(4)	O10–Tb1–N2	84.07(4)
O1–Tb1–O7	163.16(4)	O11–Tb1–O1	74.27(4)
O1–Tb1–O8	134.53(4)	O11–Tb1–O2	116.83(4)
O1–Tb1–O10	72.99(4)	O11–Tb1–O4	123.21(4)
O1–Tb1–O13	114.19(4)	O11–Tb1–O5	157.42(4)
O1–Tb1–N1	26.15(4)	O11–Tb1–O7	90.70(4)
O1–Tb1–N2	93.63(4)	O11–Tb1–O8	89.42(4)
O2–Tb1–O4	71.93(5)	O11–Tb1–O10	61.19(4)
O2–Tb1–O5	83.73(5)	O11–Tb1–O12	67.30(4)
O2–Tb1–O7	133.58(4)	O11–Tb1–O13	127.09(4)
O2–Tb1–O8	151.38(5)	O11–Tb1–N1	96.51(4)
O2–Tb1–O10	119.09(4)	O11–Tb1–N2	145.11(4)
O2–Tb1–O13	64.80(4)	O12–Tb1–O1	90.08(4)
O2–Tb1–N1	26.13(5)	O12–Tb1–O2	80.53(4)
O2–Tb1–N2	75.90(5)	O12–Tb1–O4	152.31(5)
O4–Tb1–O5	51.49(4)	O12–Tb1–O5	129.03(4)
O4–Tb1–O7	124.83(4)	O12–Tb1–O7	76.89(4)
O4–Tb1–O8	84.47(4)	O12–Tb1–O8	122.70(4)
O4–Tb1–O10	66.37(4)	O12–Tb1–O10	128.33(4)
O4–Tb1–O13	107.87(4)	O12–Tb1–O13	60.83(4)
O4–Tb1–N1	67.98(4)	O12–Tb1–N1	86.07(4)
O4–Tb1–N2	25.68(4)	O12–Tb1–N2	146.75(4)
O5–Tb1–O8	68.73(5)	O13–Tb1–N1	89.89(4)
O5–Tb1–O10	101.64(4)	O13–Tb1–N2	87.78(4)
O5–Tb1–O13	68.55(4)	N1–Tb1–N2	83.00(4)
O5–Tb1–N1	99.93(4)		
O5–Tb1–N2	25.83(4)	O11–Zn1–O12	80.45(4)
O7–Tb1–O5	80.01(4)	O11–Zn1–N4	91.28(5)
O7–Tb1–O8	50.70(4)	O11–Zn1–N5	153.66(6)
O7–Tb1–O10	106.71(4)	O12–Zn1–N4	142.71(6)
O7–Tb1–O13	68.78(4)	O12–Zn1–N5	90.56(6)
O7–Tb1–N1	157.28(4)	O1W–Zn1–O11	98.22(5)
O7–Tb1–N2	103.12(4)	O1W–Zn1–O12	106.99(5)
O8–Tb1–O10	62.08(4)	O1W–Zn1–N4	110.17(6)
O8–Tb1–O13	109.52(4)	O1W–Zn1–N5	108.09(6)
O8–Tb1–N1	150.37(4)	N5–Zn1–N4	80.94(6)
O8–Tb1–N2	75.86(4)		

Table S8. Hydrogen bonding geometrical details (distances in Å and angles in degrees) for compound $[Zn(NO_3)(L)Dy(NO_3)_2(H_2O)]$ (**1**).

D–H···A	***d*(D···A)**	**<(DHA)**
O1W−H1X···O9^{i}	2.758(2)	176
O1W−H1Y···O6^{i}	2.766(2)	163

[a] Symmetry transformations used to generate equivalent atoms: (i) -1+*x*, *y*, *z*.

Table S9. Hydrogen bonding geometrical details (distances in Å and angles in degrees) for compound $[Zn(NO_3)(L)Tb(NO_3)_2(H_2O)]$ (**2**).

D–H···A	***d*(D···A)**	**<(DHA)**
O1W−H1X···N100^{i}	2.728(2)	172
O1W−H1Y···O7^{ii}	2.7810(16)	169

[a] Symmetry transformations used to generate equivalent atoms: (i) *x*, 1+*y*, *z*; (ii) 1-*x*, 2-*y*, -*z*.

Table S10. Dysprosium geometry analysis by SHAPE[11] for $[Zn(NO_3)(L)Dy(NO_3)_2(H_2O)]$ (**1**) .

JJCU	***CCU***	**JCSAPR**	**CSAPR**	**JTCTPR**	**TCTPR**
8.990	7.201	3.965	2.611	4.275	2.543

JJCU:Capped cube
CCU: Spherical-relaxed capped cube
JCSAPR: Capped square antiprism
CSAPR: Spherical capped square antiprism
JTCTPR: Tricapped trigonal prism
TCTPR: Spherical tricapped trigonal prism

References

1. X. Lü, W. Bi, W. Chai, J. Song, J. Meng, W.-Y. Wong, W.-K. Wong and R. A. Jones, *New. J. Chem.*, 2008, **32**, 127.

2. W.-K. Lo, W.-K. Wong, W.-Y. Wong, J. Guo, K.-T. Yeung, Y.-K. Cheng, X. Yang and R. A. Jones, *Inorg. Chem.*, 2006, **45**, 9315.

3. T. Kottke and D. Stalke, *J. Appl. Crystallogr.*, 1993, **26**, 615-619.

4. *CrysalisPro Software Package, Version 1.171.34.40, Xcalibur Single Crystal CCD Diffractometer; Agilent Technologies, Yarnton, England.*, 2010.

5. *SCALE3 ABSPACK: Empirical absorption correction: CrysAlis - Software Package. Oxford Diffraction Ltd.*, 2006.

6. (a) G. M. Sheldrick, *SHELXS-97, Program for Crystal Structure Solution, University of Göttingen*, 1997; (b) G. M. Sheldrick, *Acta Cryst. A*, 2008, **64**, 112-122.

7. G. M. Sheldrick, *SHELXL-97, Program for Crystal Structure Refinement, University of Göttingen*, 1997.

8. K. Brandenburg, *DIAMOND, Version 3.2f. Crystal Impact GbR, Bonn, Germany*, 1997-2010.

9. D. Casanova, M. Llunel, P. Alemany, S. Alvarez, *Chem. Eur. J.*, 2005, **11**, 1479.